Time domain model for calculation of pure in-line vortex-induced vibrations

J. V. Ulveseter, S. Sœvik, C. M. Larsen

7491 Trondheim, Norway, Department of Marine Technology, Norwegian University of Science and Technology

Abstract

A time domain model for prediction of cross-flow vortex-induced vibrations (VIV) of slender structures with circular cross section has been under development since 2012. As an extension of this work, a time domain model for pure in-line VIV is here proposed, with the same underlying theory. The in-line force model, consisting of added mass, damping and excitation, is based on empirical data from forced oscillation tests of rigid cylinders. Damping and excitation is tuned to give the best fit of the excitation force coefficient calculated from experiments, whereas a strip theory approach is utilized to determine the force is phase with cylinder acceleration, i.e. added mass. The excitation force model represents the time varying drag force induced by alternating vortex shedding, and consists of two frequency-regions with positive excitation. Within these regions the excitation force is able to synchronize with the response vibrations, so that energy is transferred to the cylinder. Numerical simulations are performed to compare the present model with experimental results of free oscillations of rigid and flexible pipes with circular cross section, in uniform current. For the flexible cylinder case, a simple linear finite element structural model is combined with the in-line force model. The numerical simulations and the experiments are seen to match fairly well, both concerning frequency content, amplitude ratio and dominating vibration mode. Some discrepancies are observed, mostly concerning amplitude ratio. However, due to the complexity of VIV as a phenomenon, and the simplicity of the present model, it is concluded that the results are satisfactory. Consequently, this paper shows that the original idea of synchronization between excitation force and cylinder response is seen to work, not only for cross-flow VIV, but for pure in-line VIV as well.

Keywords:
Pure in-line vortex-induced vibrations, Time domain simulation, Dynamic analysis, Finite element method

1. Introduction

Vortex-induced vibrations (VIV) is a fluid-structure interaction phenomenon experienced by a large variety of slender marine structures subjected to current. Viscous effects result in flow separation and vortex shedding on the surface of the structure and in the wake, which again changes the pressure field and induces alternating lift and drag forces. As the body is free to move, vibrations may occur. VIV is a concern due to accumulation of fatigue damage and drag amplification. It is particularly important for the oil and gas industry where life time evaluation of free spanning pipelines and risers may be limited by VIV.

Research on VIV has been substantial over the last decades, both experimentally and numerically (Gabbai and Benaroya, 2005). Traditionally the cross-flow vibrations have been given most attention among researchers, as indicated in the reviews by Sarpkaya (2004) and Williamson and Govardhan (2004). This is probably due to significantly larger response amplitudes than what is observed in the in-line direction. However, in later years, in-line vibrations, and the combination of cross-flow and in-line VIV have become a larger focus area. In the review by Bearman (2011) a cylinder free to move in both transverse and in the undisturbed flow direction is compared to a cylinder constrained to vibrate in cross-flow only. On the experimental side Dahl et al. (2010) performed free oscillation tests of rigid cylinders free to vibrate in cross-flow and in-line direction, and dual resonance was observed for a wide parametric range. Aronsen (2007) did forced harmonic motion tests, where the in-line amplitude was half the cross-flow amplitude. Flow velocity, phase angle and absolute value of the amplitude were varied. However, as also discussed by Larsen (2011), the study showed large scatter indicating the importance of higher harmonics. As part of the development of the Ormen Lange field on the Norwegian continental shelf, experiments were performed, and a study of

combined in-line and cross-flow VIV for free spanning pipelines was carried out by Søreide et al. (2001) and Nielsen et al. (2002). Later, the experiments were used as basis for the PhD-thesis by Aglen (2013).

Pure in-line VIV is important for free spanning pipelines in particular. As the vibration frequency in the in-line direction is significantly higher than the vibration frequency transversely, in-line vibrations are induced at lower current velocities. This was confirmed experientially by MARINTEK as part of the Ormen Lange field development reported by Huse (2001). Designed to avoid cross-flow VIV by sufficient structural stiffness, free spanning pipelines will mainly experience accumulation of fatigue damage as a consequence of pure in-line vibrations (Larsen, 2011). In King and Prosser (1973), King (1974) and Currie and Turnbull (1987), it is emphasized that vibrations in the flow direction is important for pile-supported marine structures, braced members, jacket legs and delivery tubes, as it can cause unpleasant working environment for the staff, but also fatigue failure and structural collapse. Pure in-line VIV was also studied by Aronsen (2007) experimentally, where rigid cylinders were given a forced harmonic motion. Post-processing of the results gave a description of added mass and excitation force as function of amplitude ratio and frequency, which can be used as basis for semi-empirical prediction tools of pure in-line VIV.

Even though there exist guidelines for analysis of VIV for free spanning pipelines and risers (DNVGL, 2006, 2010), the methods are inaccurate, designed to give conservative results. Hence more specialized analysis tools are developed. Numerical solution of Navier-Stokes equation can produce a complete picture of the fluid enclosing the structure, and can hence be used to calculate VIV. As an example, Bourguet et al. (2011) uses three-dimensional direct numerical simulation to analyze a long cylindrical tensioned flexible beam at low Reynolds number. In general CFD is extremely time consuming. Thus the engineering world still rely on semi-empirical models, where the hydrodynamic VIV forces are calculated from empirical coefficients. VIVA (Triantafyllou et al., 1999), SHEAR7 (Vandiver and Li, 2005) and VIVANA (Passano et al., 2014) are all semi-empirical VIV models solving the equation of motion in frequency domain.

Marine risers and free spanning pipelines are highly non-linear structures and can undergo large deflections and experience non-linear soil-pipe interaction. The frequency response method is limited to treat a linearised problem, so time domain is the preferred solution scheme with no restrictions in the structural modelling. Lie (1995); Finn et al. (1999); Mainçon and Larsen (2011) have proposed VIV models in time domain, but none of which have been accepted as engineering tools by the industry. Also, the Van der Pol oscillator equation used to describe the fluctuating force coefficient, is utilized as basis for several numerical studies. Even for pure in-line VIV, a numerical study of a damped mass-spring model combined with a forcing term where the drag coefficient satisfies a Van der Pol equation, has been conducted (Currie and Turnbull, 1987).

During the last few years, a new semi-empirical time domain method for prediction of cross-flow VIV has been developed by Thorsen et al. (2014a). The model has later been extended, also to include in-line VIV in combination with transverse vibrations (Thorsen et al., 2014b). The way the excitation force synchronizes to the cylinder velocity to obtain lock-in, is the most remarkable aspects of this time domain model. In Thorsen et al. (2014a), the model is seen to produce realistic results for both forced and free oscillation tests of rigid cylinders, and free oscillations of flexible cylinders. Through several case studies, a high degree of realism is found for numerical simulations of flexible pipes with circular cross section in uniform and sheared current (Thorsen et al., 2014b, 2015a,b), and in oscillating flow (Thorsen et al., 2016).

In this paper, a new semi-empirical time domain model for pure in-line VIV is proposed, strongly based on the cross-flow model by Thorsen et al. (2014a). The hydrodynamic force is modelled as the sum of damping, excitation and added mass tuned to fit empirical data by Venugopal (1996) and Aronsen (2007) in the subcritical flow regime. Hydrodynamic damping is modelled as frequency-independent, which simplifies the numerical code, and still produces a damping force in acceptable agreement with Venugopal (1996). Since pure in-line VIV is characterized by two separate regions of different vortex shedding processes, two excitation force terms are utilized. They can synchronize with the cylinder velocity for a frequency range determined from forced oscillation experiments by Aronsen (2007), to provide energy to the cylinder under lock-in conditions. As the excitation force tries to synchronize with the cylinder velocity, there are time instants at which the excitation force is in phase with the acceleration. This contribution, plus an additional added mass term from potential theory of circular cylinder sections, provides the total force in phase with cylinder acceleration.

1.1. Circular cylinder subjected to current

A cylinder subjected to current will experience alternating vortex shedding for Reynolds number (Re) larger than 40 (Sumer and Fredsøe, 2006). If the cylinder is fixed, the Strouhal number ($St = \frac{f_v D}{U}$) gives the relationship between the vortex shedding frequency f_v, the diameter of the cylinder D, and the current velocity U. The Strouhal number depends on Reynolds number and the cylinder's surface roughness (Achenbach and Heinecke, 1981). At least in the subcritical flow regime, i.e. $300 < Re < 3.0 \cdot 10^5$ (Sumer and Fredsøe, 2006), the value is fairly constant and approximately equal to 0.2. The alternating vortex shedding changes the pressure distribution around the cylinder, and behaves approximately sinusoidal. This gives rise to fluctuating forces. The force component in the undisturbed current direction (in-line) is called drag, oscillating with twice the vortex shedding frequency. The component transverse to the flow direction (cross-flow) is named lift, with same frequency as the vortex shedding.

For a circular cylinder free to move, the fluctuating lift and drag forces may induce vibrations, namely vortex-induced vibrations. Experimental studies have shown that the cylinder motion can affect the vortex shedding process, and hence also the hydrodynamic forces. In cross-flow, the response frequency of the cylinder and the vortex shedding frequency can "lock" on to one another at certain conditions of mass, damping and current. This is often referred to as "lock-in" in the VIV literature, and is studied experimentally by Khalak and Williamson (1999) and Vikestad (1998), among others. As discussed by Larsen (2011), Vikestad (1998) showed that VIV under lock-in conditions is a true resonant phenomenon, where the vortex shedding frequency attaches to the natural frequency, when response dependent added mass has been accounted for.

Synchronization between response and hydrodynamic force is also experienced for vibrations in the undisturbed flow direction, studied by King and Prosser (1973), King (1974) and Currie and Turnbull (1987). The following discussion on in-line VIV is based on Sumer and Fredsøe (2006), dividing it into three separate regions, which are characterized by different vortex shedding processes. The regions are referred to as instability regions defined for an interval of reduced velocity:

$$U_r = \frac{U}{D f_n}, \tag{1}$$

where U is the current velocity, D is the cylinder diameter and f_n is the natural frequency. The first instability region is roughly for $U_r \in (1, 2.5)$. Hydrodynamically, the vibrations are a result of both alternating vortex shedding and symmetric vortex shedding caused by the motion itself. The second instability region takes place at $U_r \in (2.5, 4)$, where the alternating vortex shedding alone causes the vibrations. For both instability regions, the flow velocity is too low to induce transverse motion, hence the name pure in-line VIV. The third type of in-line VIV is seen together with cross-flow vibrations, when $U_r > 4$. The current velocities are, in this case, higher, and the cross-flow motion affects the vortex shedding inducing stronger and more orderly fashioned shedding. The result is larger response amplitudes.

For the first instability region, the in-line force oscillation frequency f_x appears approximately three times the Strouhal frequency:

$$f_x = 3St\frac{U}{D}. \tag{2}$$

As f_x approaches the natural frequency f_n, the motion amplitudes increase due to resonance. Assuming $St = 0.2$, the reduced velocity at which resonance occurs, is:

$$U_r = \frac{U}{D f_n} = \frac{U}{D\frac{3StU}{D}} \approx 1.7. \tag{3}$$

If the current velocity is further increased, f_x will, according to equation 2, move away from the natural frequency. At some point, f_x can not synchronize with the natural frequency and the vibrations die out. With no vibrations, the symmetric vortex shedding cancels and the normal alternating vortex shedding is restored. In this case, the second instability region is reached and the in-line force frequency becomes:

$$f_x = 2St\frac{U}{D}. \tag{4}$$

By still assuming $St = 0.2$, the reduced velocity at which the in-line force frequency coincides with the natural frequency, is:

$$U_r = \frac{U}{Df_n} = \frac{U}{D\frac{2StU}{D}} \approx 2.5. \tag{5}$$

2. Hydrodynamic force model

2.1. Reference frame

x is taken as the in-line direction, y is the cross-flow direction and z is the coordinate in the longitudinal direction of the circular pipe, illustrated in figure 1. $(x, y) = (0, 0)$ is chosen as the static equilibrium configuration. Hence the non-zero mean drag experienced by a circular cylinder in current is not part of the in-line force model.

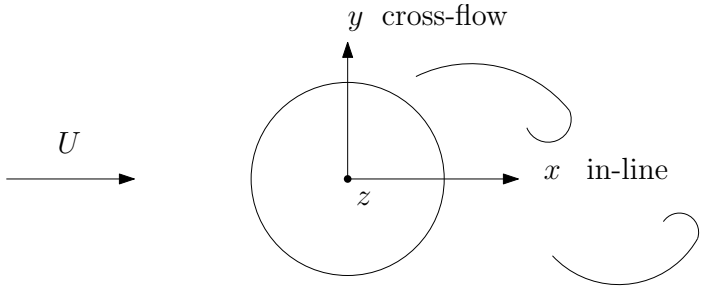

Figure 1: Illustration of reference frame for proposed model

2.2. Hydrodynamic damping model

To model hydrodynamic damping caused by the resistance experienced while moving the cylinder through fluid, the in-line damping model proposed by Venugopal (1996) is utilized. However, as this damping formulation is a function of vibration frequency, an alternative formulation is proposed, applicable for time domain simulation. For low reduced velocity, the hydrodynamic damping coefficient for a two-dimensional section in the in-line direction proposed by Venugopal (1996), is

$$c_{low} = \frac{\omega\pi\rho D^2}{2}[\frac{2\sqrt{2}}{\sqrt{Re_\omega}} + 0.25(\frac{A_x}{D})^2] + C_{il}\rho DU. \tag{6}$$

Here, ρ is the fluid density, ω the angular vibration frequency, $\frac{A_x}{D}$ the amplitude ratio, ν the kinematic viscosity and $Re_\omega = \frac{\omega D^2}{\nu}$. To fit experimental results at Reynolds number around 10^4, C_{il} was taken to be 0.19.

When solving the equation of motion using time integration, the frequency is not explicitly given and must be found as part of the solution process, as was the case for Lie (1995). Finding the frequency based on previous time history is complicated, and is the reason for the alternative damping formulation in the present work. The sum of a linear and a non-linear damping term with respect to response velocity is proposed in equation 7, where the non-linear term also depends on the amplitude of the motion:

$$F_{d,x}(t) = -\frac{1}{2}\rho DC_1U\dot{x} - \frac{1}{2}\rho A_xC_2|\dot{x}|\dot{x}. \tag{7}$$

$F_{d,x}(t)$ is the in-line damping force and A_x is the motion amplitude in the in-line direction. C_1 and C_2 are coefficients determined so that the energy dissipated per oscillation cycle is approximately the same for the two damping formulations (equation 6 and 7). By expressing the proposed damping force on non-dimensional form, i.e. $C_x = \frac{F_{x,d}(t)}{\frac{1}{2}\rho DU^2}$, the non-dimensional excitation coefficient C_e can conveniently be utilized as a measure of the energy dissipation. For harmonic in-line velocity $\omega A_x cos(\omega t)$, the excitation coefficient is defined by

$$C_e = \lim_{T\to\infty}\frac{2}{T}\int_0^T C_x(t)cos(\omega t)dt. \tag{8}$$

By inserting the proposed damping force in equation 7 into 8, the excitation coefficient can be expressed as a function of amplitude ratio and non-dimensional frequency:

$$C_e{}^{proposed} = -2\pi C_1 \hat{f}(\frac{A_x}{D}) - \frac{32}{3}\pi C_2 \hat{f}^2(\frac{A_x}{D})^3, \tag{9}$$

where the non-dimensional frequency is defined as:

$$\hat{f} = \frac{fD}{U} = \frac{\omega D}{2\pi U}. \tag{10}$$

Doing the same for the damping model by Venugopal (1996), the excitation coefficient can be written

$$C_e{}^{Venugopal} = -4\pi^3[\frac{2\sqrt{2}}{\sqrt{Re_\omega}} + 0.25(\frac{A_x}{D})^2]\hat{f}^2(\frac{A_x}{D}) - 4\pi C_{il}\hat{f}(\frac{A_x}{D}), \tag{11}$$

where $Re_\omega = 2\pi\hat{f}Re$, and Reynolds number is taken to be 10000. Then, minimizing the square of the error between the two excitation coefficients for a range of $\hat{f} \in (0.2, 0.9)$ and $0.01 < \frac{A_x}{D} < 0.20$, C_1 was found to be 0.5405, and C_2 to be 1.1824. This resulted in a mean square error of 0.93% between the two damping models.

2.3. Excitation force model

The part of the fluctuating drag force caused by the vortex shedding process is referred to as the excitation force, as it can excite structural vibrations. However, for a force to induce structural motion it has to oscillate with the same frequency as the cylinder velocity, slightly out of phase with the displacement and acceleration, for positive energy transfer from the fluid to the cylinder. In the present excitation force formulation, this is only true under lock-in conditions after reaching steady-state in the time domain simulation. Empirical data provided by Aronsen (2007) is utilized to determine the form of the excitation force, both for the first and second instability region. Aronsen (2007) performed forced harmonic oscillation experiments with rigid cylinders at Reynolds number equal to $2.4 \cdot 10^4$, and was able to calculate the excitation force coefficient as a function of non-dimensional frequency and amplitude ratio, in the undisturbed flow direction. The contour plot is shown in figure 2. At regions where the excitation force coefficient is positive the proposed excitation force model is tuned to provide energy to the cylinder. The way energy is transmitted to the cylinder at specific frequencies and motion amplitudes, is through synchronization. This mechanism was first introduced by Thorsen et al. (2014a) and will be explained in detail below.

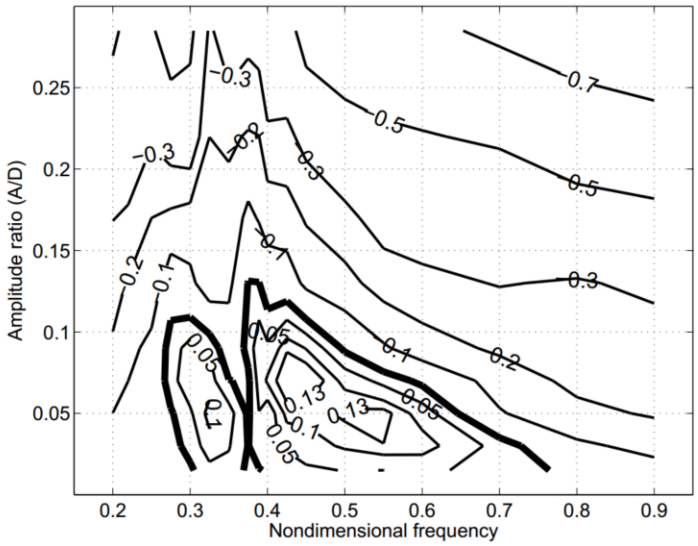

Figure 2: Contour plot of dynamic excitation coefficient in in-line direction (Aronsen, 2007)

2.3.1. Second instability region

The proposed excitation force for the second instability region is on the form:

$$F_{exc,2} = \frac{1}{2}\rho D U^2 C_{v2} cos(\Phi_{v2}), \tag{12}$$

where C_{v2} is a function of the in-line amplitude ratio, and Φ_{v2} is the instantaneous phase of the excitation force. For a harmonic oscillation, the time derivative of the instantaneous phase would be constant, i.e. $\frac{d\Phi_{v2}}{dt} = \omega_{v2}$, where ω_{v2} is the angular frequency of the excitation force. However, for the proposed formulation, this restriction is not present as $F_{exc,2}$ in equation 12 shall have the ability to synchronize with the cylinder velocity. Therefore, $\frac{d\Phi_{v2}}{dt}$ is required to be a function of the instantaneous phase of the velocity $\Phi_{\dot{x}}$ minus the instantaneous phase of the force itself:

$$\frac{\Phi_{v2}}{dt} = g_2(\theta_2), \tag{13}$$

where

$$\theta_2 = \Phi_{\dot{x}} - \Phi_{v2}. \tag{14}$$

The function g_2 in equation 13 is loosely determined from the contour plot of the excitation coefficient by Aronsen (2007) in figure 2. It is seen that the second instability region experiences positive excitation for approximately $\hat{f} \in (0.295, 0.385)$ with peak value at $\hat{f} = 0.35$, for small amplitude ratios. Mathematically,

$$\hat{f}(\theta_2) = \begin{cases} 0.35 + 0.055 sin(\theta_2) & \text{if } -\pi < \theta_2 < 0 \\ 0.35 + 0.035 sin(\theta_2) & \text{if } \pi > \theta_2 > 0 \end{cases} \tag{15}$$

is chosen to represent the synchronization range. The instantaneous phase of the force Φ_{v2} is designed to be completely in phase with the velocity at the peak value $\hat{f} = 0.35$. In the range $\hat{f} \in (0.295, 0.385)$, the excitation force can synchronize with the frequency of the cylinder velocity, but a time lag may occur. For other values of $\hat{f}$, the excitation force is not able to synchronize with the velocity.

A mathematical relation between $\frac{d\Phi_{v2}}{dt}$ and $\hat{f}$ must be established to relate equation 13 and 15. When the excitation force is to transfer energy to the cylinder, the excitation force coefficient in equation 8 must be positive. Assuming the response to be harmonic, i.e. $x = A_x sin(\omega t)$, this is only true if the force oscillates with the same frequency as the cylinder velocity. Otherwise, the integral in equation 8 is zero. This implies

$$\frac{d\Phi_{v2}}{dt} = \omega, \tag{16}$$

where ω is the frequency of the cylinder velocity, more generally written $\frac{d\Phi_{\dot{x}}}{dt}$. Combining equation 10 and 16, the following relationship between $\frac{d\Phi_{v2}}{dt}$ and $\hat{f}$ is obtained:

$$\frac{d\Phi_{v2}}{dt} = 2\pi \frac{U}{D} \hat{f}(\Phi_{\dot{x}} - \Phi_{v2}). \tag{17}$$

With $\hat{f}(\Phi_{\dot{x}} - \Phi_{v2})$ already established in equation 15, g_2 in equation 13 becomes

$$\frac{d\Phi_{v2}}{dt}(\theta_2) = \begin{cases} 2\pi \frac{U}{D}(0.35 + 0.055 sin(\theta_2)) & \text{if } -\pi < \theta_2 < 0 \\ 2\pi \frac{U}{D}(0.35 + 0.035 sin(\theta_2)) & \text{if } \pi > \theta_2 > 0. \end{cases} \tag{18}$$

The general idea is that the instantaneous frequency of the force $\frac{d\Phi_{v2}}{dt}$ can increase or decrease depending on the instantaneous phase of the force itself and the instantaneous phase of the velocity. Three cases are considered, to clarify how the synchronization works:

1. $\hat{f} \in (0.295, 0.385)$, but $\hat{f} \neq 0.35$
2. $\hat{f} = 0.35$
3. $\hat{f} \notin (0.295, 0.385)$

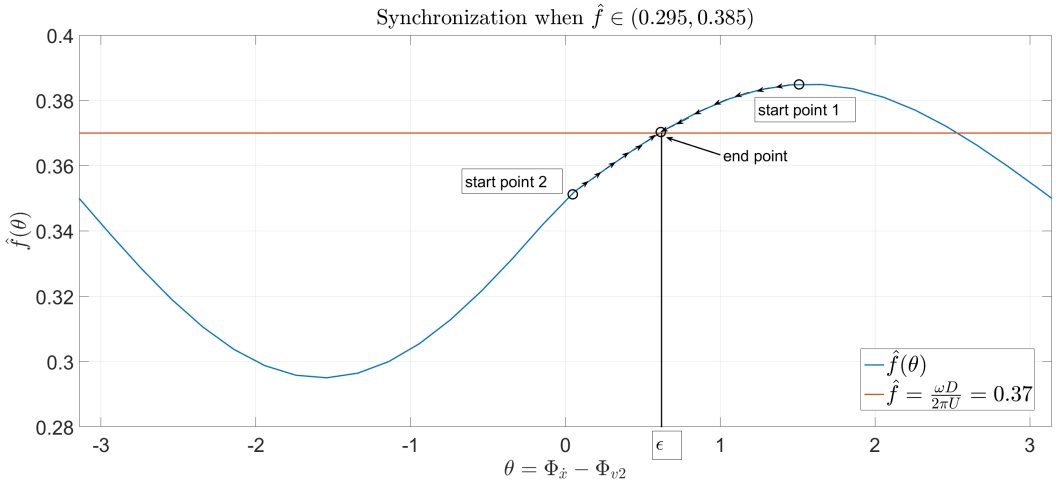

Figure 3: Synchronization for the second instability region

1. In the $\hat{f}$-range of synchronization, the instantaneous frequency of the excitation force will increase if $\frac{d\Phi_{v2}}{dt} < \omega$. This is the case for "start point 2" in figure 3. The solution reach steady-state as $\frac{d\Phi_{v2}}{dt} = \omega$, which is the "end point" in the figure. Then, $\Phi_{\dot{x}} - \Phi_{v2} = \epsilon$ and hence the excitation force can be expressed as:

$$F_{exc,2} = \frac{1}{2}\rho D U^2 C_{v2} cos(\Phi_{\dot{x}} - \epsilon) = \frac{1}{2}\rho D U^2 C_{v2} cos(\omega t - \epsilon). \tag{19}$$

   In the opposite case, when $\frac{d\Phi_{v2}}{dt} > \omega$, we are at "start point 1" in the figure. The frequency of the excitation force must decrease in order to satisfy equation 16. The solution converges towards the same "end point" as for "start point 2".
2. For example, if the cylinder velocity oscillates with a frequency equivalent to $\hat{f} = 0.35$, the red line in figure 3 is shifted 0.02 units downwards (as the figure shows synchronization when $\hat{f} = 0.37$). The new intersection between the blue and red line causes the phase shift ϵ to be zero. Hence the excitation force is completely in phase with the velocity and can be written:

$$F_{exc,2} = \frac{1}{2}\rho D U^2 C_{v2} cos(\Phi_{\dot{x}}) = \frac{1}{2}\rho D U^2 C_{v2} cos(\omega t). \tag{20}$$

3. At velocity frequencies outside the synchronization region, the red line in figure 3 has no intersection with the blue line. The result is that the frequency of the excitation force can not converge towards the frequency of the velocity.

The excitation force is dependent on the response amplitude ratio through the variable C_{v2}. Also this relationship is based on the contour plot by Aronsen (2007), in figure 2. At the chosen peak value $\hat{f} = 0.35$, the amplitude ratio where the excitation coefficient is zero, is taken to be 0.1. To generate realistic values of the excitation coefficient within the excitation region, excitation and damping are considered simultaneously. This is necessary because damping is negative excitation, 180 degrees out of phase with the cylinder velocity. Aiming for a maximum value of the excitation coefficient equal to 0.1 at $\frac{A_x}{D} = 0.06$, the functional form of C_{v2} is as illustrated in figure 4. The figure also shows how the excitation coefficient varies as function of the amplitude ratio when damping and excitation force are considered separately. It is important to note that C_{v2} is never smaller than zero. For amplitude ratios larger than what is illustrated in figure 4, C_{v2} is zero. This means that the damping force alone restricts the vibrations amplitudes to increase, which in fact assures that VIV is self-limiting.

2.3.2. First instability region

To model the excitation force giving rise to vibrations in the first instability region, the same formulation as in the second instability region is utilized. That is

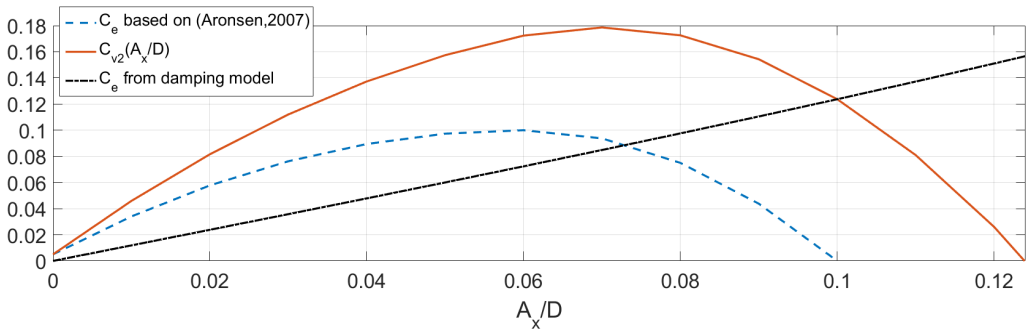

Figure 4: The functional form of C_{v2}

$$F_{exc,1} = \frac{1}{2}\rho D U^2 C_{v1} cos(\Phi_{v1}), \tag{21}$$

where C_{v1} is an amplitude dependent parameter, and Φ_{v1} is the instantaneous phase of the force. Both parameters are based on the contour plot of the excitation coefficient, by Aronsen (2007). From this, $\hat{f} \in (0.395, 0.725)$ is taken as the synchronization range for small amplitude ratios, with the excitation force completely in phase with the velocity at $\hat{f} = 0.45$. The instantaneous frequency of the excitation force is designed to satisfy

$$\frac{\Phi_{v1}}{dt} = g_1(\theta_1), \tag{22}$$

where

$$\theta_1 = \Phi_{\dot{x}} - \Phi_{v1}. \tag{23}$$

As for the second instability region a sinusoidal curve is chosen to represent the $\hat{f}$-region of positive excitation. By claiming that positive excitation only occurs when the instantaneous frequency of the excitation force is the same as the frequency of the cylinder velocity, i.e. $\frac{d\Phi_{v1}}{dt} = \omega$, g_1 in equation 22 is given by

$$\frac{d\Phi_{v1}}{dt}(\theta_1) = \begin{cases} 2\pi\frac{U}{D}(0.45 + 0.055 sin(\theta_1)) & \text{if } -\pi < \theta_1 < 0 \\ 2\pi\frac{U}{D}(0.45 + 0.275 sin(\theta_1)) & \text{if } \pi > \theta_1 > 0. \end{cases} \tag{24}$$

The relation between $\frac{A_x}{D}$ and C_{v1} is found at $\hat{f} = 0.45$, where the excitation is completely in phase with the cylinder velocity. C_{v1} is chosen so that the excitation coefficient, considering both damping and excitation, is equal to zero at $\frac{A_x}{D} = 0.12$, and for all larger amplitude ratios. The maximum value of the excitation coefficient is taken to be 0.14 at $\frac{A_x}{D} = 0.07$. This is illustrated in figure 5.

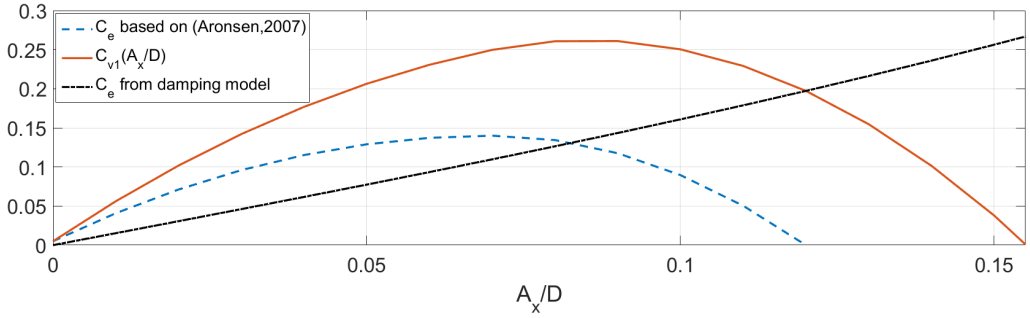

Figure 5: The functional form of C_{v1}

2.4. Determination of amplitude and the instantaneous phase of cylinder velocity during time integration

From the previous discussion it is clear that both damping and excitation force depend on response amplitude. This information is extracted as part of the time integration process, assuming the response to be narrow-banded. The motion amplitude is updated for every zero-crossing of the response velocity, according to

$$A_x = \frac{1}{2}\int_{t_1}^{t_2} |\dot{x}|dt = \frac{1}{2}|x(t_2) - x(t_1)|, \tag{25}$$

where the time instant at most recent zero-crossing t_1 and t_2 are illustrated in figure 6. Equation 25 is solved by numerical integration, and the procedure is equivalent to what was done by Thorsen et al. (2014a).

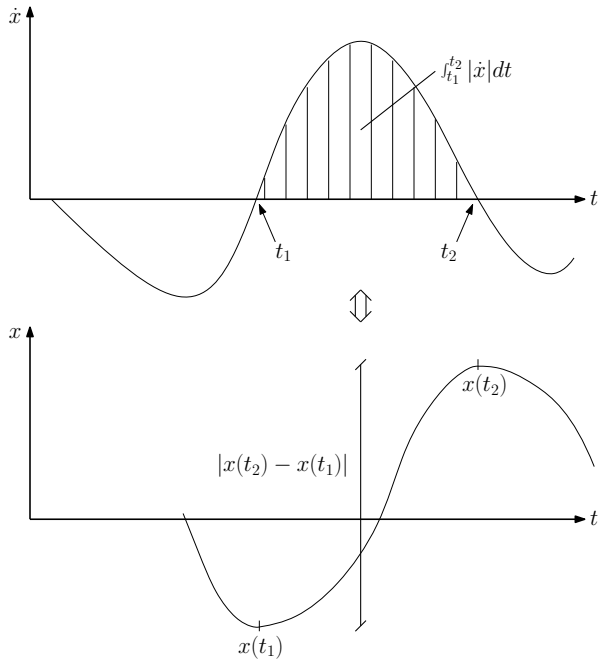

Figure 6: Illustration of equation 25

The response amplitude is, according to equation 25, only updated at time instants where the velocity is zero. In-between these zero-crossings, the amplitude is constant. Consequently, the amplitude input to the force model consists of abrupt changes when reaching a zero-crossing of the velocity. This may induce transient effects and stability problems in the time integration process. This is why Thorsen et al. (2016) proposed a smoothed amplitude response curve, which converges towards the solution obtained by equation 25, when the vibrations reach steady-state. The same smoothing technique is utilized in the proposed in-line VIV model. The smoothed amplitude A_x^* is defined by

$$\frac{dA_x^*}{dt} = k_A(A_x - A_x^*), \tag{26}$$

where k_A is a small constant. Equation 26 is solved numerically. The fluctuations of A_x and A_x^* is illustrated in figure 7, for a free oscillation test of a rigid cylinder. The first 10% of the total simulation time is used to increase the current velocity linearly from zero to a prescribed value, explaining the large number of cycles before steady-state is reached.

The excitation force synchronization is dependent on the instantaneous phase of the cylinder velocity $\Phi_{\dot{x}}$, as understood from equation 14 and 23. This is a quantity that must be extracted from the time domain simulation at every time step, to update the frequency of the excitation force as often as possible. The phase portrait concept is utilized for this purpose, described by Thorsen et al. (2014a) in the cross-flow direction.

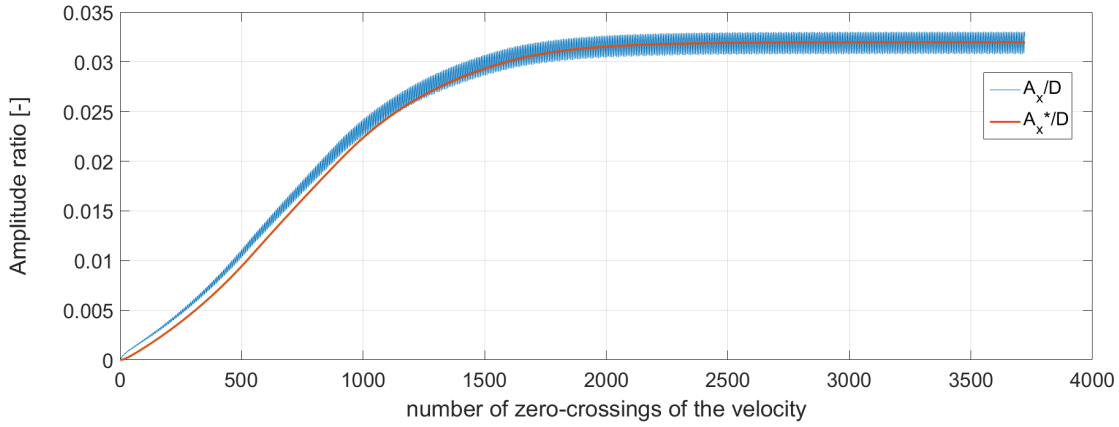

Figure 7: Smoothed response amplitude A_x^* vs A_x, for $k_A = 0.05$ in equation 26

2.5. Total time domain model

The total hydrodynamic force is taken as the sum of damping, excitation and added mass. The latter is caused by the cylinder acceleration disturbing the fluid and hence the pressure on the structure. Two-dimensional added mass for a circular cylinder is utilized. However, as the excitation force continuously tries to synchronize with the cylinder velocity, there are time instants where it may contribute with a force component in phase with acceleration. Hence both the excitation force and added mass give force in phase with cylinder acceleration. The total pure in-line VIV force for a one degree of freedom system may be written

$$F_x(t) = -\frac{1}{2}\rho D C_1 U \dot{x} - \frac{1}{2}\rho A_x C_2 |\dot{x}|\dot{x} + \frac{1}{2}\rho D U^2 C_{v1} cos\Phi_{v1} + \frac{1}{2}\rho D U^2 C_{v2} cos\Phi_{v2} - \rho\frac{\pi D^2}{4}\ddot{x}, \tag{27}$$

where the two first terms are the damping forces, third and fourth term are the excitation forces for first and second instability regions respectively, and the last term is the force proportional to the cylinder acceleration due to two-dimensional added mass.

Equation 27 is combined with a structural model to predict pure in-line VIV response. To simulate elastically mounted rigid cylinders subjected to small current velocity, the in-line motion is taken as the only degree of freedom. Structural mass M, stiffness K_s and damping C_s is provided as input to the model, and stepwise numerical time integration is performed to solve the dynamic equilibrium equation

$$M\ddot{x}(t) + C_s\dot{x}(t) + K_s x(t) = F_x(t). \tag{28}$$

For a flexible pipe, a finite element model gives the structural stiffness, damping and mass properties. Beam elements with four degrees of freedom are utilized. The hydrodynamic force is calculated at every translation degree of freedom along the structure, based on the response amplitude at the corresponding node. The instantaneous phase of the excitation forces are taken to be randomly distributed in the initial stage of the simulation at every node, to avoid initial (and unphysical) correlation over the whole span length. Instead correlation is built up as the current velocity is slowly increased to the input value. Since the hydrodynamic force is calculated at two-dimensional sections, only the finite element structural model communicates the three-dimensional effects in the present formulation. The equation of motion is

$$\mathbf{M}\ddot{\mathbf{x}}(t) + \mathbf{C_s}\dot{\mathbf{x}}(t) + \mathbf{K_s}\mathbf{x}(t) = \mathbf{F_x}(t), \tag{29}$$

where $\mathbf{M}$ is the consistent mass matrix plus constant added mass ($\rho\frac{\pi D^2}{4}$), $\mathbf{K_s}$ is the structural stiffness matrix due to bending stiffness and pipe tension, $\mathbf{C_s}$ is the structural damping matrix, $\mathbf{F_x}(t)$ is the hydrodynamic force vector without constant added mass, and $\mathbf{x}(t)$ is the response vector containing translations and rotations.

The equation of motion is, for both rigid and flexible pipes, solved by Newmark-β stepwise time integration, described by Langen and Sigbjörnsson (1979). The parameters are chosen in agreement with the

method of constant average acceleration, i.e. $\lambda = 0.5$ and $\beta = 0.25$. $\lambda = 0.5$ provides no artificial damping, and the method is unconditionally stable.

3. Results

3.1. Forced oscillations - Rigid pipe

By simulating the behaviour of the proposed in-line force model when a rigid cylinder is forced to move harmonically in the undisturbed flow direction, the excitation force coefficient and added mass coefficient per unit length can be found for a chosen frequency and amplitude. Such a simulation is presented in the following, with properties given in table 1. The simulations were performed for amplitude and frequency of the forced harmonic motion in the intervals $\hat{f} \in (0.2, 0.9)$ and $0.01 < \frac{A_x}{D} < 0.30$, and contour plots of the force coefficients were created. The excitation force coefficient and added mass coefficient are given by

$$C_e = \lim_{T\to\infty} \frac{2}{T} \int_0^T C^e_{x,tot}(t) cos(\omega t) dt, \tag{30}$$

where

$$C^e_{x,tot}(t) = \frac{F_x(t)}{\frac{1}{2}\rho D U^2}, \tag{31}$$

and

$$C_a = \lim_{T\to\infty} \frac{2}{T} \int_0^T C^a_{x,tot}(t) sin(\omega t) dt, \tag{32}$$

where

$$C^a_{x,tot}(t) = \frac{F_x(t)}{\frac{\pi D^2}{4}\rho\omega^2 A_x}. \tag{33}$$

Table 1: Properties of forced oscillation test Phase I (Aronsen, 2007)

Name	**Symbol**	**Size**	**Dimension**
Diameter	D	0.150	[m]
Water density	ρ	1000	[kg/m^3]
Current velocity	U	0.175	[m/s]
Reynolds number	Re	$2.4 \cdot 10^4$	[-]

The uncertainty in the result, presented in figure 9 and 10, is considered to be low, but not necessarily negligible. Whereas the definition of both coefficients are taken to be an integral over an infinite time period, the numerical simulation were performed over a finite time period. Also, the in-line force is observed to be extremely sensitive when it is not allowed to affect the response, which is constrained to be harmonic. This is because the force maxima are so peaked that a very small time step is needed to perform the numerical integration accurately. This effect is illustrated in figure 8. The final simulation was performed with 350 time periods and 500 time steps per cycle, which gave a small scatter of the excitation coefficient for two specific points in the $\hat{f}\frac{A_x}{D}$-plane.

From the contour plot of the excitation force coefficient (figure 9), good agreement between the simulation and the experimental results by Aronsen (2007), is observed. As previously described, the two excitation forces, and partly the damping model, are constructed to recreate this figure, and hence the agreement is expected. For both excitation regions, the amplitude at which C_e becomes zero, the frequency at which the maximum energy is transferred to the cylinder, and the value of C_e in the excitation regions, are consistent with what was aimed at. Outside the excitation regions, only the damping model gives a force contribution in phase with the cylinder velocity. This contribution is negative, as damping transfers energy from the cylinder to the surrounding fluid. Also in the damping region, the value of the excitation coefficient compares well with Aronsen (2007). At least for $\frac{A_x}{D} < 0.15$, which is most important because pure in-line VIV rarely exceed this

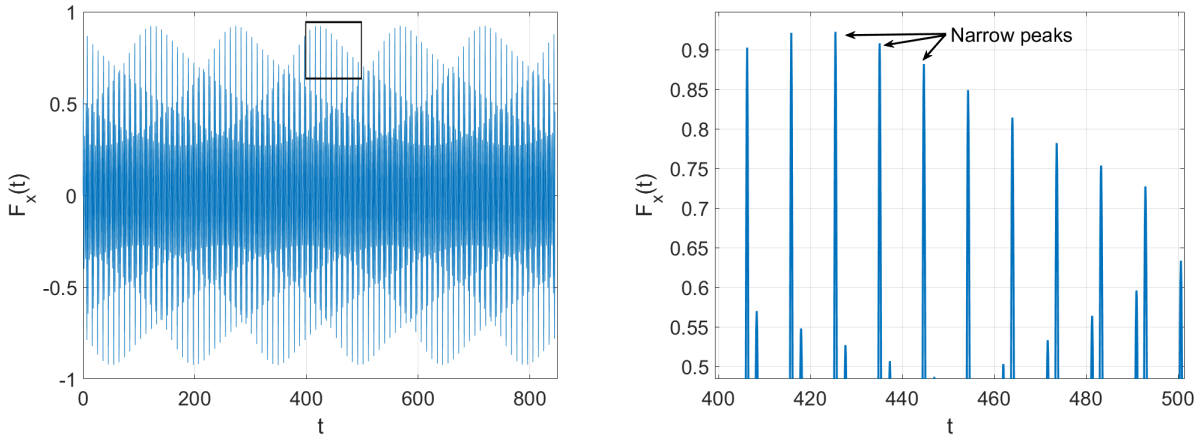

(a) Total hydrodynamic force for $(\hat{f}, \frac{A_x}{D}) = (0.355, 0.03)$

(b) Zoomed in on narrow peaks

Figure 8: Force response for simulation of rigid pipe

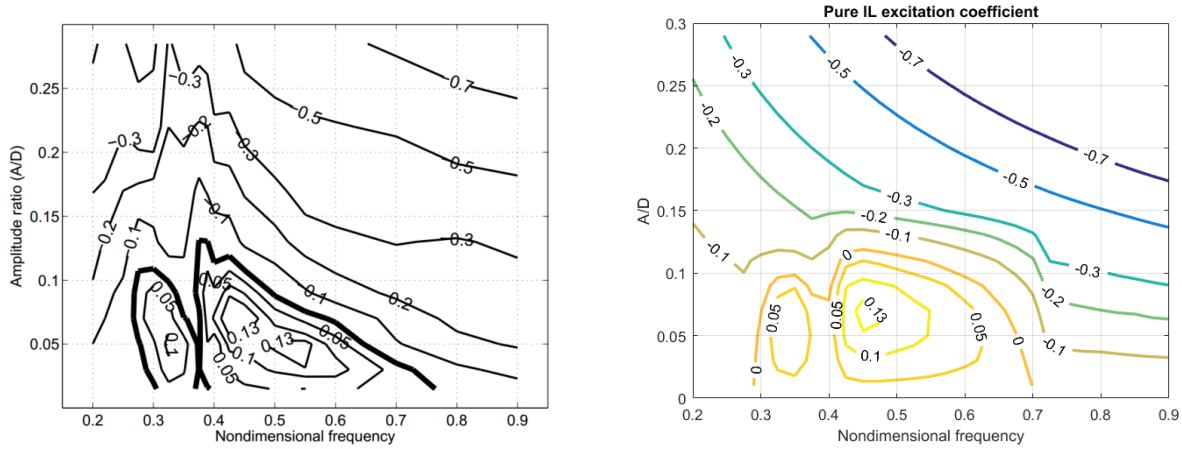

(a) Contour plot of excitation coefficient by Aronsen (2007)

(b) Simulated contour plot of excitation coefficient

Figure 9: Excitation coefficient C_e

amplitude limit. However, for the first instability region, some discrepancies are seen. The present damping and excitation models are not capable of producing the almost straight line dividing positive and negative excitation for $\hat{f} \in (0.4, 0.75)$. Instead, the simulated excitation force coefficient has a more rounded shape, causing too large excitation at large amplitude ratios, but smaller values than desired at low amplitudes. This might indicate that the way synchronization is utilized in the excitation force is not sufficient to produce the wanted shape more accurately.

The simulated added mass coefficient, which illustrates the force component in phase with acceleration, does not compare so well with Aronsen (2007), in figure 10. The trend that C_a decreases for low $\hat{f}$ is somehow captured by the simulation, and hence it is concluded that the added mass model consisting of two-dimensional added mass from potential strip theory and the acceleration component from the excitation force, is not unphysical. Actually, it looks like the simulated added mass coefficient is a squeezed version of the experimental result, over a narrower $\hat{f}$-region, for amplitude ratios below 0.15. However, by looking at figure 11, this is not completely the case. For $\frac{A_x}{D} > 0.15$, the excitation force is zero, and hence only the two-dimensional added mass from strip theory produces a force component in phase with acceleration, giving a value of approximately one for C_a.

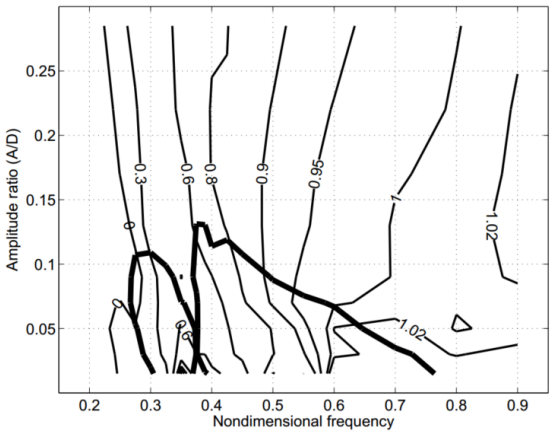

(a) Contour plot of added mass coefficient by Aronsen (2007)

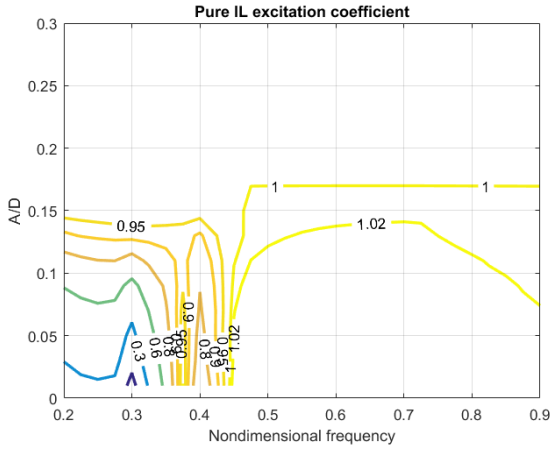

(b) Simulated contour plot of added mass coefficient

Figure 10: Added mass coefficient C_a

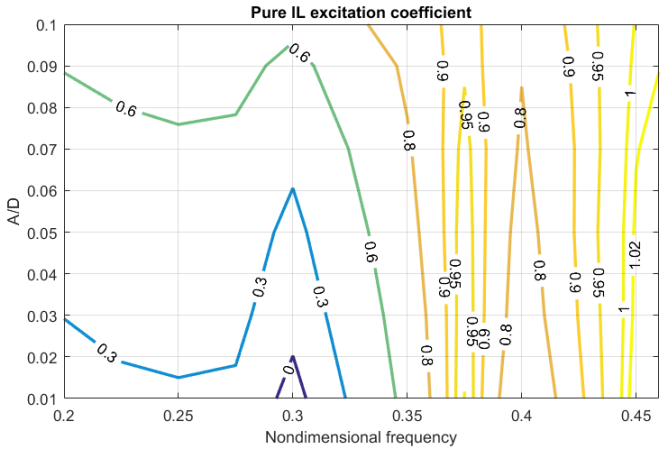

Figure 11: Zoomed version of the simulated C_a contour plot in figure 10

For a frequency domain VIV model one may assume that the response frequency agrees with an eigenfrequency:

$$f_n = \frac{1}{2\pi}\sqrt{\frac{k}{m+m_a}} \tag{34}$$

where k is the stiffness, m is the dry mass and m_a is the added mass. From this, a correct added mass representation is crucial for the response frequency predictions. This is the case for the semi-empirical VIV program VIVANA, where iterations are performed to make sure the added mass is consistent with the present vibration frequency. If not, the oscillation frequency will not be estimated correctly. In time domain, the frequency of the oscillation builds up as part of the solution. So how important is added mass for the present model? Looking at all the test series where pure in-line VIV response was predicted for flexible pipelines (presented in figure 15, 16 and 17) the agreement between simulated and experimental frequency is very good. Of course, if the mass ratio is large, the added mass influence is reduced, which can explain the result. However, the point is that added mass might not directly affect the response frequency in time domain as it does in frequency domain, and therefore a small mismatch in simulated and experimental added mass may not be a major limitation of the present model.

3.2. Free oscillations - Rigid pipe

To simulate the response of a rigid cylinder subjected to uniform current the equation of motion is solved by stepwise numerical time integration, as explained in section 2.5. Such simulations were performed for a set of current velocities spanning from $U_r = 0.1 - 6.0$. The response output was compared to results of free oscillation tests of a rigid cylinder constrained only to move in the in-line direction, reported by Johansen (2004). Physical data is provided in table 2.

Table 2: Properties of free oscillation test of rigid cylinder

Name	**Symbol**	**Size**	**Dimension**
Diameter	D	0.08	[m]
Water density	ρ	1000	[kg/m^3]
Dry mass	$m_{dry} = m^* \rho \frac{\pi D^2}{4}$	$10.51 \rho \frac{\pi D^2}{4}$	[kg/m]
Damping ratio	$\xi = \frac{c_s}{c_{cr}}$	0.0081	[-]
Natural period	T_p	0.0803	[s]

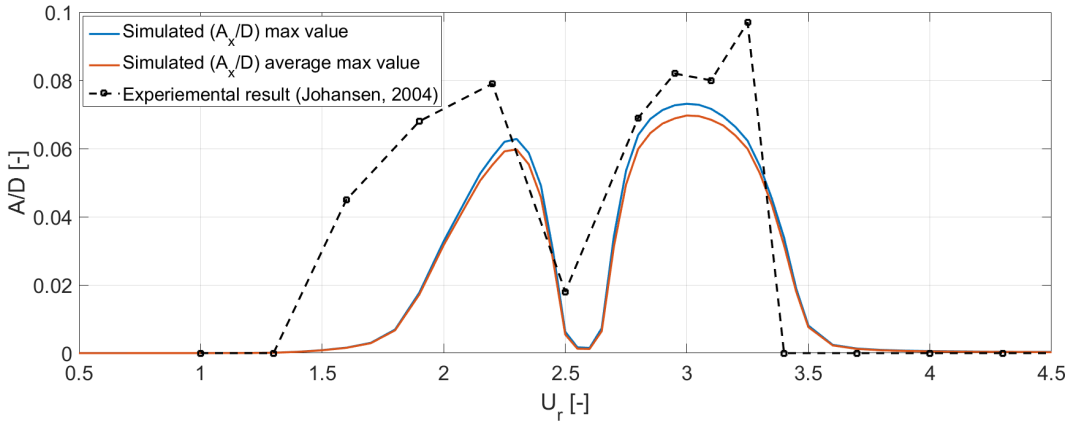

Figure 12: Comparison of simulated and experimental value of in-line amplitude ratio as function of reduced velocity

Looking at the amplitude ratio as function of the reduced velocity in figure 12, the simulations produce values in the same order of magnitude as the experiment. A slight underestimation is seen for more or less the whole reduced velocity range. In the first instability region, the simulated amplitude does not build up before $U_r \in (1.5, 2.0)$, whereas the experiments show significant response already at $U_r = 1.5$. This might be a consequence of the shortcomings of the excitation coefficient in the first instability region, as addressed previously. As structural damping is accounted for in the numerical simulation, the excitation force might be too small to induce vibrations at large non-dimensional frequencies, i.e. $\hat{f} \in (0.55, 0.7)$, which is equivalent to low reduced velocities. This is illustrated in figure 13, which also shows that the maximum simulated response amplitudes occur around $\hat{f} = 0.35$ and $\hat{f} = 0.45$, where the excitation force is in complete phase with the velocity. This is according to the expectations.

The general trend that the amplitude ratio is predicted to be non-conservative might also be influenced by Reynolds number, which is not a parameter in the proposed VIV model. A discussion of Re-dependency for VIV on flexible pipes was carried out by Swithenbank et al. (2008) and on rigid cylinders by Govardhan and Williamson (2006). The latter concluded that the peak amplitudes of VIV response for $Re \in (500, 33000)$ depend on the parameter according to $log(0.41 Re^{0.36})$. In other words, the amplitudes increase with increasing Reynolds number. However, the study was performed by considering cross-flow motion and zero damping, which is not applicable to the present study. If the same trends are valid for in-line VIV with small damping ratios, the consequence is as follows: By assuming the kinematic viscosity to be $\nu = 1.0 \cdot 10^{-6}$ m^2/s, the experiments in figure 12 are performed with Reynolds number less than $2.4 \cdot 10^4$ for $U_r < 3$. Hence the experimental results should, according to Govardhan and Williamson (2006), give slightly smaller amplitudes than the simulation for $U_r < 3$. This is the opposite of what is seen for the first instability region. For the

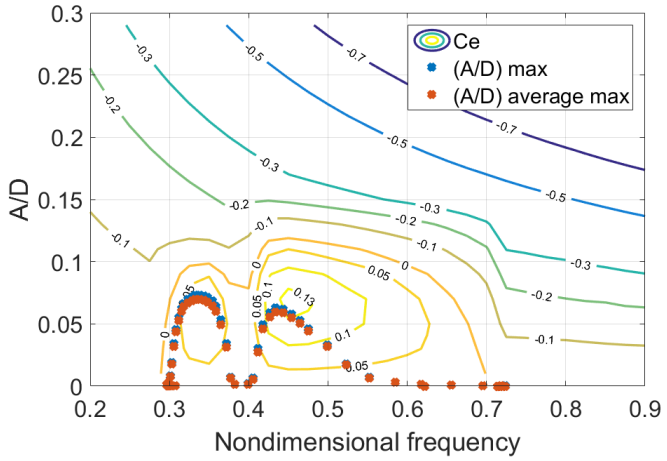

Figure 13: Simulated in-line VIV response for rigid pipe compared to simulated contour plot of excitation force coefficient

second instability region, considering $U_r > 3$, the simulated amplitudes are slightly underestimated, which coincide with the observed behaviour.

3.3. Free oscillations - Flexible pipe

The main reason why pure in-line VIV is a concern is fatigue damage of free spanning pipelines subjected to low current velocities. Such slender marine structures may be modelled as flexible pipes, applying the finite element method for structural modelling (see section 2.5). The hydrodynamic force model is tuned to work optimally for forced oscillation tests of rigid cylinders. Hence, it is not obvious that the proposed model is capable of reliable predictions for flexible beams. This is examined in the following, where the simulations are based on three specific configurations of a model scale Ormen Lange pipeline towed at MARINTEK's ocean basin laboratory. The pipeline was free to move both in cross-flow and in-line, and because the proposed model predicts pure in-line VIV, simulations were performed for low current velocities at which cross-flow VIV was not present. A lot of configurations were tested as part of the Ormen Lange project. In the present study, simulations were performed for what was referred to as test series 10, 42 and 75. This was also done by Passano et al. (2010) using VIVANA as the VIV analysis tool. The main difference between the test series is the free span length, varied by putting on clamps at specific positions along the pipe. Properties of the tests are presented in table 3, together with schematic illustrations in figure 14.

Table 3: Properties of free oscillation tests of flexible pipes (Passano et al., 2010), (Aglen, 2013)

Parameter	**Test series 10**	**Test series 42**	**Test series 75**	**Dimension**
Length, L	11.413	11.413	11.413	[m]
Free span length, L_f	11.413	4.729	3.421	[m]
Diameter, D	0.0326	0.0326	0.03504	[m]
Water density, ρ	1000	1000	1000	[kg/m^3]
Dry mass, m_{dry}	1.147	1.147	1.307	[kg/m]
Damping ratio, ξ	0.004	0.004	0.004	[-]
Bending stiffness, EI	0.203	0.203	0.203	[kNm^2]
Static tension, T	67.8	51.5	50.0	[N]
Number of clamps, N_c	0	6	16	[-]
Clamp stiffness, k_c	-	$9 \cdot 10^6$	$5 \cdot 10^6$	[N/m]

In the numerical simulation, and in figure 14, the clamps were modelled as vertical springs since the vertical motion was not restrained completely in the experiment. The test set-up applied a truss girder as support structure for the pipe with a horizontal spring in one end (z-direction) to keep the tension approximately constant. In the numerical simulation, four degrees of freedom beam elements were utilized,

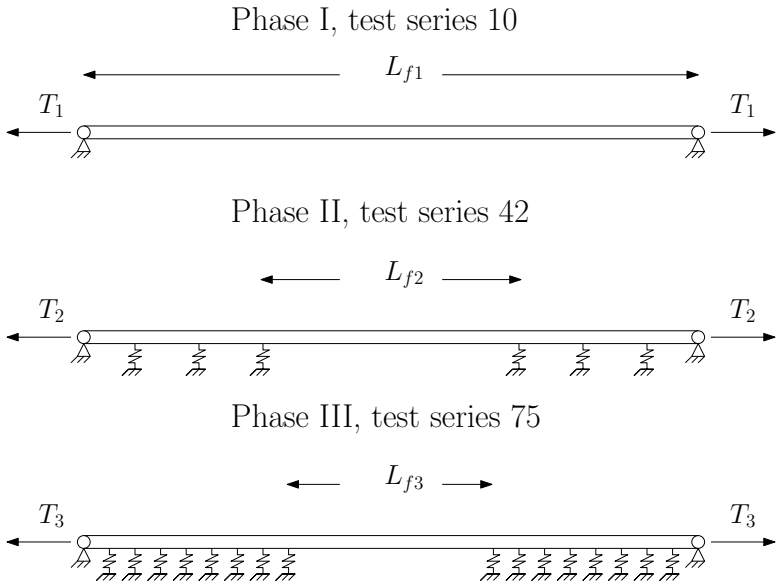

Figure 14: Illustration of the Ormen Lange experiments

not including axial degrees of freedom. This is due to large axial stiffness combined with small response amplitudes keeping the axial displacements at a negligible level. From this, the end conditions were assumed to be simply supported, with all movements restrained except for rotation about the y-axis, and with a constant tension contributing to the stiffness of the system.

All three simulated series produce results that compare very well with the measurements (see figure 15, 16 and 17), especially with respect to oscillation frequency and mode number. The frequency is slightly underpredicted for test series 42 and 75. This will lead to a non-conservative fatigue life estimate. Since the frequency compares more or less perfectly for test series 10 the underprediction of oscillation frequency is not a general trend of the proposed model. Nevertheless, the discrepancies for test series 42 and 75 are considered to be too small to play a significant role. The dominating response mode is identical for all simulations and experiments. This is important for correct stress distribution over the length of the pipeline, which relates to the fatigue life through the SN curve. Number of cycles until failure N, at dynamic stress range S, for a structure built by a material with parameters K and m, is given by $N = KS^{-m}$. The amplitude ratio is not as accurately predicted by the proposed model. However, all simulated values are in a realistic range of what can be excepted for pure in-line VIV. Discrepancies may be a consequence of uncertainty in measurements/post-processing of experimental results, and that the simple form of the proposed model is not able to capture the complete picture of the energy transfer between the fluid and the pipe. Looking at test series 75, the motion amplitudes are slightly overestimated for current velocity in the upper range, i.e. $U \in (0.16, 0.24)$ m/s, but lower than the experimental value for smaller velocities. As for the free oscillation test of the rigid cylinder, this may be due to the rounded shape of the excitation coefficient for the first instability region, which is a problem already addressed.

An interesting observation is that the simulated results plotted in the contour plot of the excitation coefficient shows that the average maximum amplitude ratios follow the $C_e = 0$ curve more closely than the absolute maxima (figure 18). The excitation coefficient is a measure of the average energy transfer to the system, and so it makes sense that the average value of the amplitude ratio agrees better with the curve. For $\hat{f}$-values in the range of synchronization, the corresponding amplitude ratios exceed the $C_e = 0$ curve. For a flexible pipeline, there will be a global energy balance between the fluid and the pipe itself. For mode one response, the energy input from the fluid at the pipe sections closest to the boundaries is transferred to the midsection of the pipeline and back to the fluid, inducing larger response amplitudes than what is observed for a rigid cylinder (Larsen, 2011). Hence, that the amplitude ratio exceeds the values at which $C_e = 0$ is according to theory. The whole study indicates that the hydrodynamic force model is applicable to multi degree of freedom systems, even though the empirical input is based on forced motion of rigid cylinders.

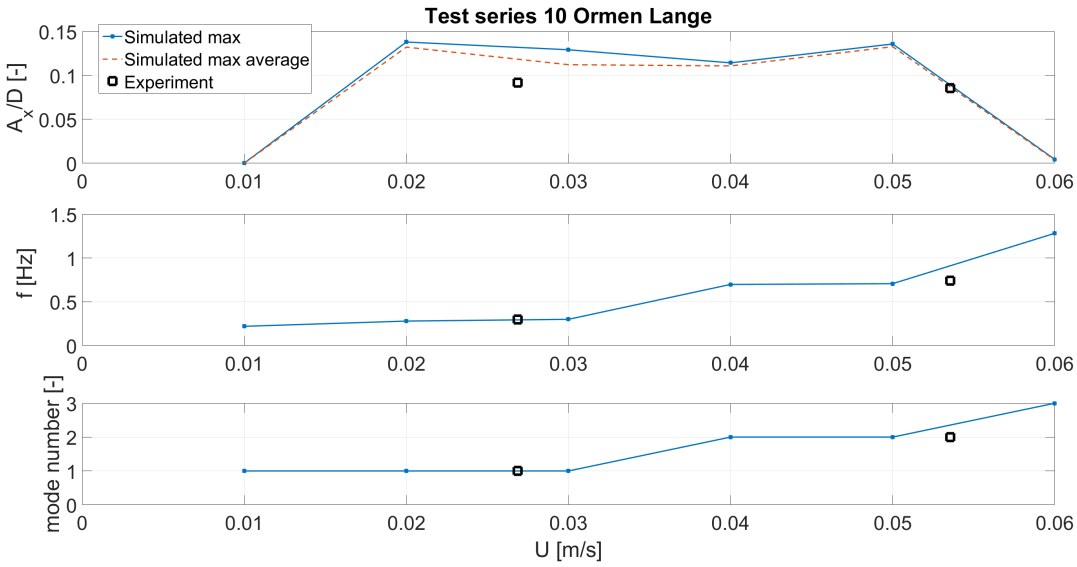

Figure 15: Amplitude ratio, frequency and mode number for Test series 10

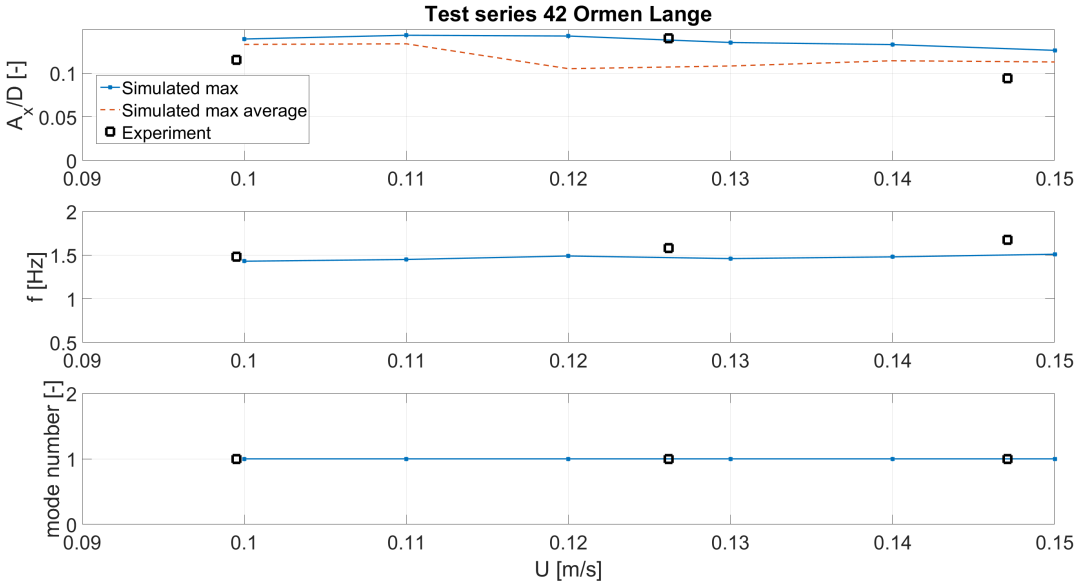

Figure 16: Amplitude ratio, frequency and mode number for Test series 42

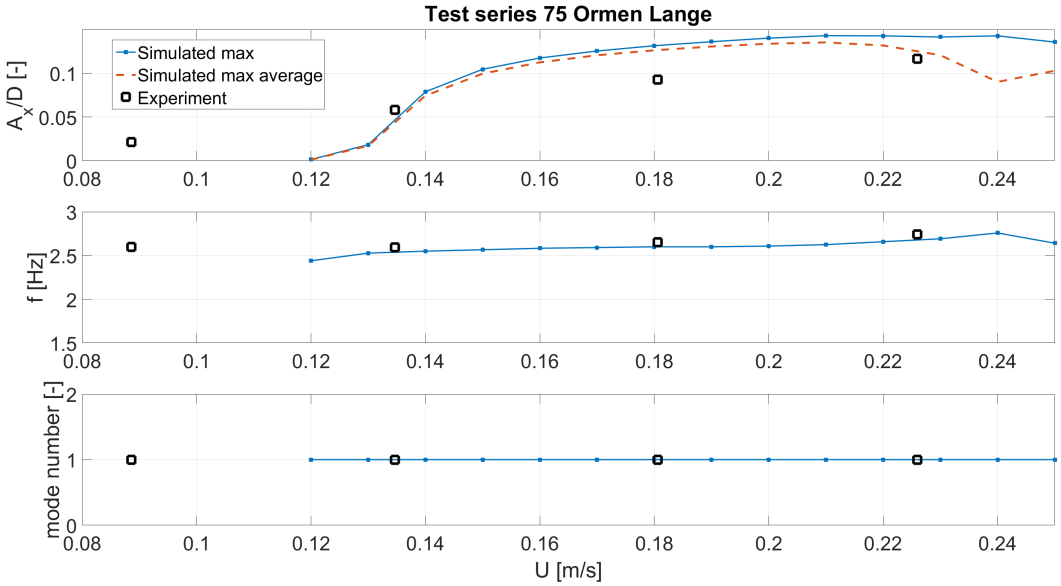

Figure 17: Amplitude ratio, frequency and mode number for Test series 75

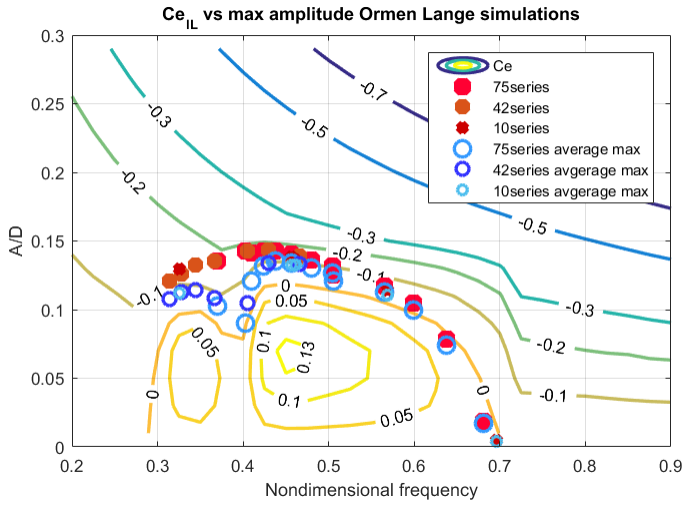

Figure 18: Simulated results of Ormen Lange compared to the contour plot of the excitation coefficient

4. Conclusion

A time domain model for the prediction of pure in-line VIV response of slender structures with circular cross section has been presented. Based on empirical data of the excitation force coefficient and hydrodynamic damping for different frequencies and amplitude ratios, a hydrodynamic force model is established consisting of damping, added mass and excitation terms. The latter is most important as it is designed to capture the nature of lock-in. For two separate frequency-regions, the excitation force can synchronize with the cylinder velocity causing structural vibrations. The hydrodynamic force model is seen to produce the frequency and amplitude variation of the empirically calculated dynamic excitation coefficient sufficiently good when a cylinder is forced to move harmonically. For the added mass coefficient, the agreement between experiments and simulations is not so good, but the model is still able to predict dominating oscillating frequency close to measurements. When combined with simple structural models, simulations compare well with free oscillation experiments of rigid and flexible pipes.

A possible improvement of the work is to tune model parameters so that both excitation coefficient and added mass coefficient fit better with measurements. Also, Reynolds number dependency is not taken into account in the proposed work. For more realistic modelling of real-size oil and gas pipes, empirical data at higher flow regimes than subcritical is needed for parameter tuning.

As the equation of motion is solved in time domain, there are few restrictions in modelling possibilities. For example arbitrary current profiles, time-varying in-flow and non-linear structural models can be simulated. Also VIV in combination with wave-induced motion is possible to simulate if the in-line VIV model is tuned to work together with Morion's equation. Since pure in-line VIV is of concern for free spanning pipelines, future work may focus on combining the hydrodynamic force model with realistic pipeline models taking into account non-linear seabed-pipe interaction both with respect to soil stiffness and soil damping. By implementing the proposed hydrodynamic force model into a sophisticated finite element software, such analyses can be performed more accurately and with less effort than what is possible using MATLAB, which is the current state.

Acknowledgement

The authors would like to thank Halvor Lie and Elizabeth Passano at MARINTEK for their contribution to the present work. Their experimental and numerical expertise related to VIV has been important for finding relevant experiments to compare the hydrodynamic force model with, and choosing parameters in the numerical study. A great thanks is also addressed to Kristoffer Aronsen who has contributed by providing experimental results from his research on pure in-line VIV. For the Ormen Lange experiments Ida Aglen played an important role in providing relevant data, which was approved by Finn Gunnar Nielsen. This was very helpful in the development of the present work. A valuable contribution has come from Mats Thorsen who has, through conversations regarding all aspects of the proposed in-line VIV model, shared his wisdom and ideas. This has been highly appreciated.

References

Achenbach, E., Heinecke, E., 1981. On vortex shedding from smooth and rough cylinders in the range of reynolds numbers $6x10^3$ to $5x10^6$. J. Fluid Mech. 109, 239–251.

Aglen, I. M., 2013. Viv in free spanning pipelines. Ph.D. thesis, Norwegian University of Science and Technology (NTNU).

Aronsen, K., 2007. An experimental investigation of in-line and combined in-line and cross-flow vortex induced vibrations. Ph.D. thesis, Norwegian University of Science and Technology (NTNU).

Bearman, P. W., 2011. Circular cylinder wakes and vortex-induced vibrations. Journal of Fluids and Structures 27, 648–658.

Bourguet, R., Karniadakis, G. E., Triantafyllou, M. S., 2011. Vortex-induced vibrations of a long flexible cylinder in shear flow. J. Fluid Mech. 677, 342–382.

Currie, I. G., Turnbull, D. H., 1987. Streamwise oscillations of cylinders near the critical reynolds number. Journal of Fluids and Structures 1, 185–196.

Dahl, J. M., Hover, F. S., Triantafyllou, M. S., Oakley, O. H., 2010. Dual resonance in vortex-induced vibrations at subcritical and supercritical reynolds numbers. J. Fluid Mech. 643, 395–424.

DNVGL, 2006. Free Spanning Pipelines, DNV-RP-F105.

DNVGL, 2010. Riser Fatigue, DNV-RP-F204.

Finn, L., Lambrakos, K., Maher, J., 1999. Time domain prediction of riser viv. In: 4th International Conference on Advances in Riser Technologies.

Gabbai, R. D., Benaroya, H., 2005. An overview of modeling and experiements of vortex-induced vibration of circular cylinders. Journal of Sound and Vibration 282, 575–616.

Govardhan, R. N., Williamson, C. H. K., 2006. Defining the 'modified griffin plot' in vortex-induced vibration: revealing the effect of reynolds number using controlled damping. J. Fluid Mech. 561, 147–180.

Huse, E., 2001. Ormen lange 3d model tests. Tech. rep., MARINTEK, Norwegian Marine Technology Research Institute.

Johansen, T., 2004. Hydrodynamic coefficients for vortex-induced vibrations in current direction. Master's thesis, Norwegian University of Science and Technology (NTNU).

Khalak, A., Williamson, C. H. K., 1999. Motions, forces and mode transitions in vortex-induced vibrations at low mass-damping. Journal of Fluids and Structures 13, 813–851.

King, R., 1974. Vortex excited structural oscillations of a circular cylinder in steady currents. In: Offshore Technology Conference.

King, R., Prosser, M. J., 1973. On vortex excitation of model piles in water. Journal of Sound and Vibration 29, 169–188.

Langen, I., Sigbjörnsson, R., 1979. Dynamic Analysis of Constructions (Dynamisk Analyse av Konstruksjoner). Tapir.

Larsen, C. M., oct 2011. Vortex induced vibrations viv, a short and incomplete introduction to fundamental concepts. Department of Marine Technology NTNU.

Lie, H., 1995. A time domain model for simulation of vortex induced vibratins on a cable. In: Proceedings of Sixth International Conference on Flow Induced Vibrations.

Mainçon, P., Larsen, C. M., 2011. Towards a time-domain finite element analysis of vortex induced vibrations. In: Proceedings of the ASME 2011 30th International Conference on Ocean, Offshore and Arctic Engineering OMAE2011.

Nielsen, F. G., Søreide, T. H., Kvarme, S. T., 2002. Viv response of long free spanning pipelines. In: Proceedings of OMAE'02 21st International Conference on Offshore Mechanics and Arctic Engineering.

Passano, E., Larsen, C. M., Lie, H., Wu, J., 2014. Vivana Theory Manual, Release 4.2.

Passano, E., Larsen, C. M., Wu, J., 2010. Viv of free spanning pipelines: Comparison of response from semi-empirical code to model tests. In: Proceedings of the ASME 29th International Conference on Ocean, Offshore and Arctic Engineering OMAE2010.

Sarpkaya, T., 2004. A critical review of the intrinsic nature of vortex-induced vibrations. Journal of Fluids and Structures 19, 389–447.

Søreide, T. H., Paulsen, G., Nielsen, F. G., 2001. Parameter study of long free spans. In: Proceedings of the Eleventh (2001) International Offshore and Polar Engineering Conference.

Sumer, B. M., Fredsøe, J., 2006. Hydrodynamics around cylindrical structures. Vol. 26. World Scientific Publishing Co. Pte. Ltd.

Swithenbank, S. B., Vandiver, J. K., Larsen, C. M., Lie, H., 2008. Reynolds number dependence of flexible cylinder viv response data. In: Proceedings of the ASME 27th International Conference on Offshore Mechanics and Arctic Engineering OMAE2008.

Thorsen, M., Sævik, S., Larsen, C., 2014a. A simplified method for time domain simulation of cross-flow vortex-induced vibrations. Jornal of Fluids and Structures 49, 135–148.

Thorsen, M. J., Sævik, S., Larsen, C. M., 2014b. Time domain simulation of cross-flow and in-line vortex-induced vibrations. In: Proceedings of the 9th International Conference on Structural Dynamics, EURODYN 2014.

Thorsen, M. J., Sævik, S., Larsen, C. M., 2015a. Fatuge damage from time domain simulation of combined in-line and cross-flow vortex-induced vibrations. Marine Structures 41, 200–222.

Thorsen, M. J., Sævik, S., Larsen, C. M., 2015b. Time domain simulation of vortex-induced vibrations based on phase-coupled oscillator synchronization. In: Proceedings of the ASME 2015 34th International Conference on Ocean, Offshore and Arctic Engineering OMAE2015.

Thorsen, M. J., Sævik, S., Larsen, C. M., 2016. Time domain simulation of vortex-induced vibrations in stationary and oscillating flows. Journal of Fluids and Structures 61, 1–19.

Triantafyllou, M., Triantafyllou, G., Tein, Y., Ambrose, B. D., 1999. Pragmatic riser viv analysis. In: Offshore Technology Conference.

Vandiver, J. K., Li, L., 2005. SHEAR7 V4.4 Program Theoretical Manual.

Venugopal, M., 1996. Damping and response prediction of a flexible cylinder in a current. Ph.D. thesis, Massachusetts Institute of Technology (MIT).

Vikestad, K., 1998. Multi-frequency response of a cylinder subjected to vortex shedding and support motions. Ph.D. thesis, Norwegian University of Science and Technology (NTNU).

Williamson, C. H. K., Govardhan, R., 2004. Vortex-induced vibrations. Annual Review of Fluid Mechanics 36, 413–455.